Optical Engineering

OpticalEngineering.SPIEDigitalLibrary.org

Multiple snapshot colored compressive spectral imager

Claudia V. Correa
Carlos A. Hinojosa
Gonzalo R. Arce
Henry Arguello

SPIE.

Claudia V. Correa, Carlos A. Hinojosa, Gonzalo R. Arce, Henry Arguello, "Multiple snapshot colored compressive spectral imager," *Opt. Eng.* **56**(4), 041309 (2016), doi: 10.1117/1.OE.56.4.041309.

Downloaded From: http://opticalengineering.spiedigitallibrary.org/ on 03/03/2017 Terms of Use: http://spiedigitallibrary.org/ss/termsofuse.aspx

Multiple snapshot colored compressive spectral imager

Claudia V. Correa,[a] Carlos A. Hinojosa,[b] Gonzalo R. Arce,[a] and Henry Arguello[b,*]
[a]University of Delaware, Department of Electrical and Computer Engineering, 140 Evans Hall, Newark, Delaware 19716, United States
[b]Universidad Industrial de Santander, Carrera 27 Calle 9, Bucaramanga 680002, Colombia

Abstract. The snapshot colored compressive spectral imager (SCCSI) is a recent compressive spectral imaging (CSI) architecture that senses the spatial and spectral information of a scene in a single snapshot by means of a colored mosaic FPA detector and a dispersive element. Commonly, CSI architectures allow multiple snapshot acquisition, yielding improved reconstructions of spatially detailed and spectrally rich scenes. Each snapshot is captured employing a different coding pattern. In principle, SCCSI does not admit multiple snapshots since the pixelated tiling of optical filters is directly attached to the detector. This paper extends the concept of SCCSI to a system admitting multiple snapshot acquisition by rotating the dispersive element, so the dispersed spatio-spectral source is coded and integrated at different detector pixels in each rotation. Thus, a different set of coded projections is captured using the same optical components of the original architecture. The mathematical model of the multishot SCCSI system is presented along with several simulations. Results show that a gain up to 7 dB of peak signal-to-noise ratio is achieved when four SCCSI snapshots are compared to a single snapshot reconstruction. Furthermore, a gain up to 5 dB is obtained with respect to state-of-the-art architecture, the multishot CASSI. © *2016 Society of Photo-Optical Instrumentation Engineers (SPIE)* [DOI: 10.1117/1.OE.56.4.041309]

Keywords: compressive spectral imaging; compressive sampling; colored mosaic detectors; optical filters.

Paper 161372SSP received Sep. 1, 2016; accepted for publication Nov. 22, 2016; published online Dec. 21, 2016.

1 Introduction

Spectral imaging collects two-dimensional (2-D) spatial data at specific wavebands across the electromagnetic spectrum. These data sets are regarded as three-dimensional (3-D) images, where two of the coordinates correspond to the spatial domain and the third one represents the spectral wavelengths. In general, traditional spectral imaging methods require scanning a number of zones linearly in proportion to the desired spatial or spectral resolution, which, in turn, increases acquisition times. On the other hand, snapshot spectral imaging captures the spatial and spectral information of a scene by mapping all the voxels of the spectral data cube into different regions of a large focal plane array (FPA).[1–3] Furthermore, spectral imaging using Fabry–Perot filters or colored mosaic FPA detectors captures small subsets of spectral bands by assigning a particular spectral response to each FPA pixel, so a specific range of wavelengths is captured.[4–7] In general, these traditional techniques require all voxels of the 3-D scene to be sensed. Then, as spatial or spectral resolution increases, the number of voxels to be sensed increases proportionally, leading to an increment in the cost of sensing, storing, and transmitting a spectral image acquired using these methods. Compressive spectral imaging (CSI), on the other hand, recently emerged as a spectral imaging approach that captures 2-D coded and dispersed projections rather than direct measurements of the voxels. Then, compressive sampling-based computational algorithms are employed to recover the 3-D source from the 2-D measurement set. Although CSI devices are also snapshot-based, the number of samples acquired is far less than those sensed with traditional snapshot methods, which leads to faster sampling.[8,9]

To acquire the compressed measurements, CSI devices use a coding optical element and a dispersive element to obtain the spectral components of the image. For instance, one of the most representative CSI architectures is the coded aperture snapshot spectral imager (CASSI).[10,11] In particular, CASSI uses a coded aperture as the coding optical element that is a block–unblock lithographic mask or a spatial light modulator, in which each spatial position is either a transparent or opaque element that blocks or lets all the spectral bands of the image pass through, so the source is uniformly encoded across a range of wavelengths.[8] After the coding process, the spectral image is dispersed by a prism before being integrated at the FPA detector. Although the CASSI system achieves acceptable spatial and spectral resolutions, this system entails the use of additional lenses that result in several imaging planes.[8]

A more recent CSI architecture is the snapshot colored compressive spectral imager (SCCSI), which engages the resolution capabilities of the CASSI system and the compactness of Fabry–Perot-based architectures.[12] In this optical architecture, the coding element is a color-patterned FPA detector that implements a tiling layout of different optical filters, i.e., colors. This detector design can be built using thin film coating and lithographic techniques.[13–17] More specifically, in SCCSI, the spectral image $\mathbf{F}$, with L spectral bands, $N \times N$ pixels of spatial resolution, and entries denoted as $F_{m,n,k}$, is first dispersed by a prism. In the dispersion operation, each spectral band is horizontally sheared, as shown in Fig. 1. Then, the dispersed source is encoded by the array of optical filters $\mathbf{C}$, whose entries are indexed as $C_{m,n,k}$. In particular, each spatial location $C_{m,n}$ is assigned a spectral response that filters the incident light in that particular position. Furthermore, there exists one-to-one matching between

*Address all correspondence to: Henry Arguello, E-mail: henarfu@uis.edu.co

0091-3286/2016/$25.00 © 2016 SPIE

Downloaded From: http://opticalengineering.spiedigitallibrary.org/ on 03/03/2017 Terms of Use: http://spiedigitallibrary.org/ss/termsofuse.aspx

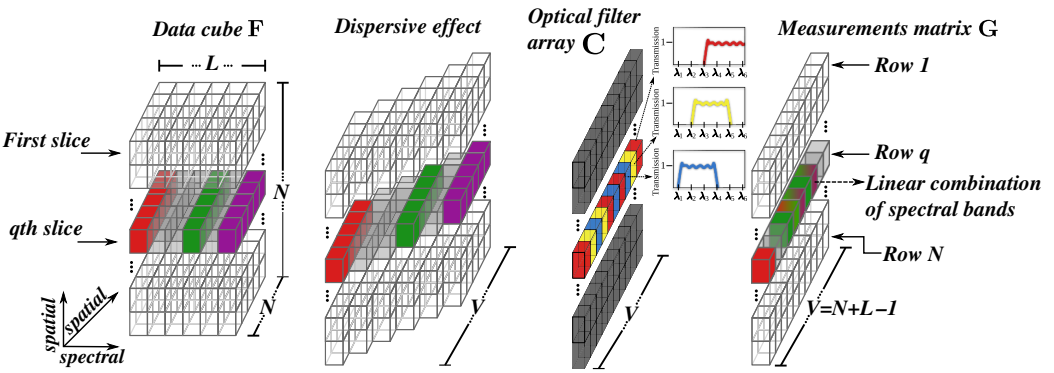

Fig. 1 Schematic representation of the SCCSI sensing process.

the elements of the optical filter array and those of the FPA. Finally, the encoded and dispersed source is integrated along the spectral range sensitivity of the detector resulting in a $N \times V$ set of measurements $\mathbf{G}$, with $V = N + L - 1$.

In general, CSI projections can be written in matrix notation as $\mathbf{g} = \mathbf{Hf} = \mathbf{H\Psi\theta}$, where $\mathbf{g} \in \mathbb{R}^{NV}$ is the measurement set in vector form and $\mathbf{f} = \mathbf{\Psi\theta} \in \mathbb{R}^{N^2L}$ is a vector representation of the source $\mathbf{F}$, which is assumed to be sparse in some basis $\mathbf{\Psi}$. Moreover, $\mathbf{H}$ is known as the system sensing matrix; its entries are determined by the coding optical element, and its structure accounts for the dispersion effect.[8] CSI spectral image recovery consists of finding a S-sparse representation of $\mathbf{f}$, $\boldsymbol{\theta}$ in a given basis $\mathbf{\Psi}$, where S represents the number of nonzero coefficients in $\boldsymbol{\theta}$. The sparse representation can be obtained by minimizing the $\ell_2 - \ell_1$ cost function given by $\|\mathbf{g} - \mathbf{A\theta}\|_2 + \tau\|\boldsymbol{\theta}\|_1$, where τ is a regularization constant.[8,18] In general, CSI establishes that $v \gtrsim S\log(N^2L) \ll N^2L$ compressed projections are sufficient to recover $\mathbf{f}$ with high probability. For instance, in CASSI and SCCSI, $N \times V$ projections are captured in a single snapshot, yielding a compression ratio of $NV/N^2L \approx 1/L$. Although it has been shown that a single snapshot provides accurate reconstructions,[12] spatially detailed or spectrally rich scenes may require additional measurements. For this reason, CSI devices enable multiple snapshot acquisition to improve the spectral image reconstructions.[8,19,20] In the multishot approach, each snapshot employs a different coding pattern, so different measurements are captured each time.[21] Such multiple measurements can be attained using a digital micromirror device (DMD) that changes the block–unblock patterns before each snapshot and remains fixed during the integration time of the detector.[22–24] In the multiple snapshot approach, the compression ratio is increased according to the expression K/L, where K is the number of acquired shots.

Given that in SCCSI the pixelated tiling of optical filters is directly attached to the detector, it is not possible to implement multiple coding patterns. Therefore, this paper extends the concept of SCCSI to a system admitting multiple measurement shots by rotating the dispersive element such that the dispersed spatio-spectral source is coded/filtered and integrated at different detector regions in each rotation. This approach allows the acquisition of a different set of coded projections on each measurement shot using the same optical components of the original SCCSI architecture, in which the dispersive element is the only moving component.[25]

This paper is organized as follows: first, the mathematical model of the SCCSI multishot system is described along with the discrete mathematical model and a matrix representation of the sensing process behind SCCSI. Finally, simulations are developed to test the performance of the proposed system.

2 Multiple Snapshot Colored Compressive Spectral Imager

Given that the encoding pattern is directly attached to the detector, each snapshot in SCCSI can be attained by rotating the dispersive element at different angles, which results in a variation of the dispersion direction, so the dispersed spectral image is encoded and integrated at different regions of the FPA detector. In addition, since the optical filters are randomly distributed within the optical filter array, different coded and dispersed scene projections are acquired depending on the rotation angle of the prism, assuming that the scene remains static during the acquisition process. Figure 2 shows a schematic representation of the proposed multishot SCCSI system. As observed, multiple snapshots can be achieved using the same components of the original SCCSI architecture, keeping low hardware complexity[12] and the dispersive element as the only moving part of the system.

2.1 *Multiple Snapshot Colored Compressive Spectral Imager Continuous Model*

When white light passes through the prism, all the wavelengths are refracted at different angles because the propagation velocity of each wavelength is different for each dispersive media whose refractive index is distinct for each color. Depending on the prism positioning with respect to the reference coordinate system, the spectrum is dispersed in a determined direction.[26] Thus, the proposed multishot SCCSI approach considers the prism rotation in the xy-plane, as shown in Fig. 2, such that the spectral source is dispersed in different directions according to the rotation angle and impinges onto different detector regions. Therefore, at each snapshot, the prism is rotated to a specific angle and remains fixed during the integration time of the detector.

The spatio-spectral source density $f_0(x, y, \lambda)$, where x, y index the spatial coordinates and λ indexes the spectral dimension, is first dispersed by the dispersive element, yielding $f_1(x, y, \lambda)$. The resulting dispersed field can be expressed as

Downloaded From: http://opticalengineering.spiedigitallibrary.org/ on 03/03/2017 Terms of Use: http://spiedigitallibrary.org/ss/termsofuse.aspx

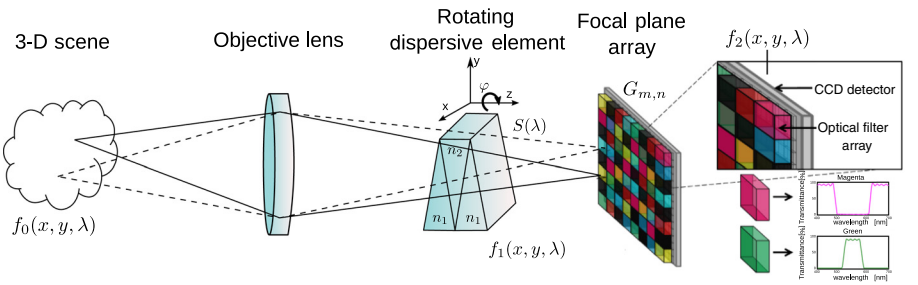

Fig. 2 Schematic representation of the SCCSI.[12] Note that the prism is the only moving part of the architecture, and the rotation angle φ determines the dispersion direction.

$$f_1(x,y,\lambda) = \iint f_0(x',y',\lambda)h(x'-x-S(\lambda),y'-y)\mathrm{d}x'\mathrm{d}y', \tag{1}$$

where $h(\cdot)$ is the optical impulse response of the system and $S(\lambda)$ is the dispersion function of the dispersive element, which operates along the x-axis. After being dispersed, the source is encoded by the colored detector, which can be modeled as an array of optical filters $C(x,y,\lambda)$, followed by an irradiance detector. Each spatial location of $\mathbf{C}$ is associated with a specific spectral response that modulates the incident light in that particular position, and the energy impinging one detector pixel is affected by just one optical filter element given that there is one-to-one matching between the elements of the color filter array and those of the FPA. Because the dispersion direction changes with the rotation angle of the prism, the dispersed source is encoded at different regions of the detector, hence the coded and dispersed source impinging on the detector can be written as

$$f_2^{\varphi}(x,y,\lambda) = f_1(x,y,\lambda)C^{\varphi}(x,y,\lambda), \tag{2}$$

where $C^{\varphi}(x,y,\lambda)$ denotes the region of the optical filter array, in which the encoded and dispersed source is integrated when the prism is positioned at the angle φ. The compressive measurements for each rotation angle, denoted as $g^{\varphi}(x,y)$, are finally obtained by the integration of the field $f_2^{\varphi}(x,y,\lambda)$ over the spectral range sensitivity of the detector (Λ). More specifically, using Eqs. (1) and (2), the SCCSI compressive measurements for a rotation angle φ are given by

$$\begin{aligned} g^{\varphi}(x,y) &= \int_{\Lambda} f_2^{\varphi}(x,y,\lambda)\mathrm{d}\lambda \\ &= \int_{\Lambda}\iint f_0(x',y',\lambda)h[x'-x-S(\lambda),y'-y] \\ &\quad \times C^{\varphi}(x,y,\lambda)\mathrm{d}x'\mathrm{d}y'\mathrm{d}\lambda. \end{aligned} \tag{3}$$

2.2 *Multiple Snapshot Colored Compressive Spectral Imager Discrete Model*

The input spatio-spectral scene can be represented as a discrete data cube $\mathbf{F} \in \mathbb{R}^{N\times N\times L}$, with L spectral bands of $N\times N$ pixels. Each source voxel is indexed as $F_{m,n,k}$, where $m,n = 0,\ldots,N-1$ are the discrete indices for the spatial dimensions and $k = 0,\ldots,L-1$ indexes the spectral bands. In addition, the pixel pitch of the detector determines the discrete representation of the optical filter array $\mathbf{C}_{m,n,k}$.[12]

Using these discrete representations, SCCSI projections can be written as

$$G_{m,n} = \sum_{k=0}^{L-1} F_{m,(n-k),k}C_{m,n,k}. \tag{4}$$

Equation (4) presents the coded projections captured in the single snapshot SCCSI, in which it is assumed that the rotation angle is set to $\varphi = 0$ deg. In this case, the dispersion occurs along the x-axis resulting in a $N\times V$ measurement set.

Let us consider the rotation of the dispersive element in the $x-y$-plane. In principle, there are no restrictions to the rotation angle φ. Hence, several FPA measurement snapshots can be acquired depending on the precision of the rotating device. However, for most values of φ, the energy of a single voxel might not impinge into a single detector pixel; instead, it will split into two or more regions. For simplicity purposes, this work is limited to four snapshots corresponding to $\varphi = \{0,90,180,270\}$ deg, given that for these rotation angles it can be assumed that the energy of a voxel is captured in a single detector pixel, assuming squared FPA pixels. The sensing mechanism for these angles is shown in Fig. 3. As previously mentioned, a 0-deg rotation corresponds to the single snapshot SCCSI case, in which the input data cube $\mathbf{F}$ is horizontally sheared along the x-axis. Similarly, a prism rotation of $\varphi = 180$ deg results in a horizontal shearing in the opposite direction of the previous case. Furthermore, both of these angles result in a $N\times V$ measurement set. On the other hand, when the prism is rotated $\varphi = 90$ deg, $\mathbf{F}$ is vertically dispersed along the y-axis, resulting in a $V\times N$ coded projections set. Finally, a rotation of $\varphi = 270$ deg results in a vertical dispersion along the y-axis in the opposite direction of the 90-deg case.

Following the SCCSI sensing process, the dispersed source is then coded by the optical filter array $\mathbf{C}$ and finally integrated at the FPA detector. Moreover, the optical filter array and FPA detector must be large enough to capture the dispersed information from different rotation angles. Specifically, for a $N\times N\times L$ data cube, the detector and optical filter array dimensions should be $W\times W$, with $W = N+2L-2$. Each rotation involves a different encoding pattern since the incoming energy is captured by different regions of the detector.

Mathematically, the discrete outputs for $\varphi = \{0,90,180,270\}$ deg are given by

$$G_{m,n}^{0} = \sum_{k=0}^{L-1} F_{m',(n'-k),k}C_{m,n,k}, \quad G_{m,n}^{90} = \sum_{k=0}^{L-1} F_{(m'+k),n',k}C_{m,n,k}, \tag{5}$$

Downloaded From: http://opticalengineering.spiedigitallibrary.org/ on 03/03/2017 Terms of Use: http://spiedigitallibrary.org/ss/termsofuse.aspx

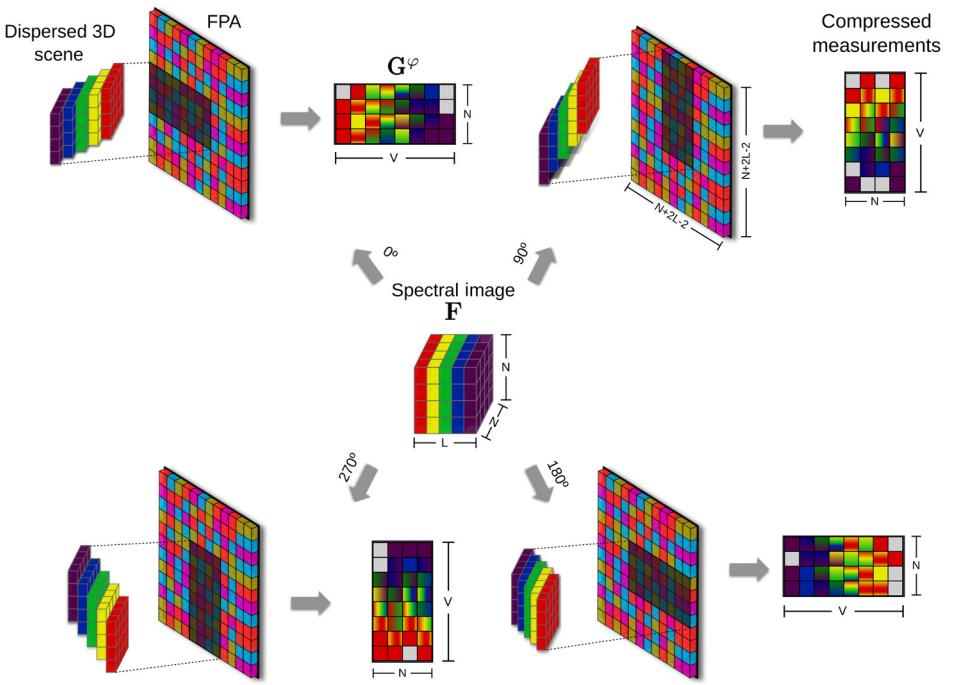

Fig. 3 Illustration of the multishot SCCSI sensing scheme. Initially, the $N \times N \times L$ spectral data cube is dispersed by the prism according to the dispersive function $S(\lambda)$, and the prism rotation angle is given by φ. This angle determines the direction in which the dispersion occurs. Then, the optical filter array $\mathbf{C}$ encodes the dispersed light before being integrated by the FPA detector.

$$G_{m,n}^{180} = \sum_{k=0}^{L-1} F_{m',(n'+k),k} C_{m,n,k}, \quad G_{m,n}^{270} = \sum_{k=0}^{L-1} F_{(m'-k),n',k} C_{m,n,k}, \tag{6}$$

where $G_{m,n}^{\varphi}$ is the intensity measured at the (m,n)'th pixel of the detector when the prism is rotated φ degrees, with $m' = m - (L-1)$ and $n' = n - (L-1)$.

2.3 *Matrix Model*

The set of compressive measurements from Eqs. (5) and (6) can be expressed in vector notation as $\mathbf{g}^{\varphi}$, so each capture of the multishot SCCSI system can be modeled by

$$\mathbf{g}^{\varphi} = \mathbf{H}^{\varphi}\mathbf{f}, \tag{7}$$

for $\varphi \in \{0, 90, 180, 270\}$, where $\mathbf{f}$ is the vector representation of the spatio-spectral input source $\mathbf{F}$ and $\mathbf{H}^{\varphi}$ is the SCCSI sensing matrix for each rotation angle φ. More specifically, $\mathbf{H}^{\varphi}$ is a $NV \times N^2 L$ sparse matrix whose nonzero entries are determined by the spectral responses of the optical filters in the optical filter array, and its structure accounts for the effect of dispersion given by rotating the prism to an angle φ. Furthermore, the entries of each $\mathbf{H}^{\varphi}$ depend on the optical filter array positions that affect the incident energy on each case, as shown in Fig. 3.

Taking this into account, the entries of the j'th row of the sensing matrix $\mathbf{H}^{\varphi}$ for $\varphi \in \{0, 90, 180, 270\}$ can be written as

$$(\mathbf{h}_j)_{\ell}^{0} = \begin{cases} (\mathbf{c}_k)_{(L-1)(w+2\lfloor \ell'/N \rfloor + 1)+j+k(2L-2),} & \text{if } \ell - k\tilde{N} = j \\ 0, & \text{otherwise} \end{cases}, \tag{8}$$

$$(\mathbf{h}_j)_{\ell}^{90} = \begin{cases} (\mathbf{c}_k)_{(L-1)(w+\lfloor \ell'/N \rfloor)+j,} & \text{if } (L-1)(\lfloor \ell'/N \rfloor + 1) + \ell - k(N^2+1) = j \\ 0, & \text{otherwise} \end{cases}, \tag{9}$$

$$(\mathbf{h}_j)_{\ell}^{180} = \begin{cases} (\mathbf{c}_k)_{(L-1)(w+2\lfloor \ell'/N \rfloor - (N-1))+j-k(2L-2),} & \text{if } \ell - k\hat{N} + N(L-1) = j \\ 0, & \text{otherwise} \end{cases}, \tag{10}$$

$$(\mathbf{h}_j)_{\ell}^{270} = \begin{cases} (\mathbf{c}_k)_{(L-1)(w+\lfloor \ell'/N \rfloor + 1)+j,} & \text{if } (L-1)(\lfloor \ell'/N \rfloor) + \ell - k(N^2-1) = j \\ 0, & \text{otherwise} \end{cases}, \tag{11}$$

Downloaded From: http://opticalengineering.spiedigitallibrary.org/ on 03/03/2017 Terms of Use: http://spiedigitallibrary.org/ss/termsofuse.aspx

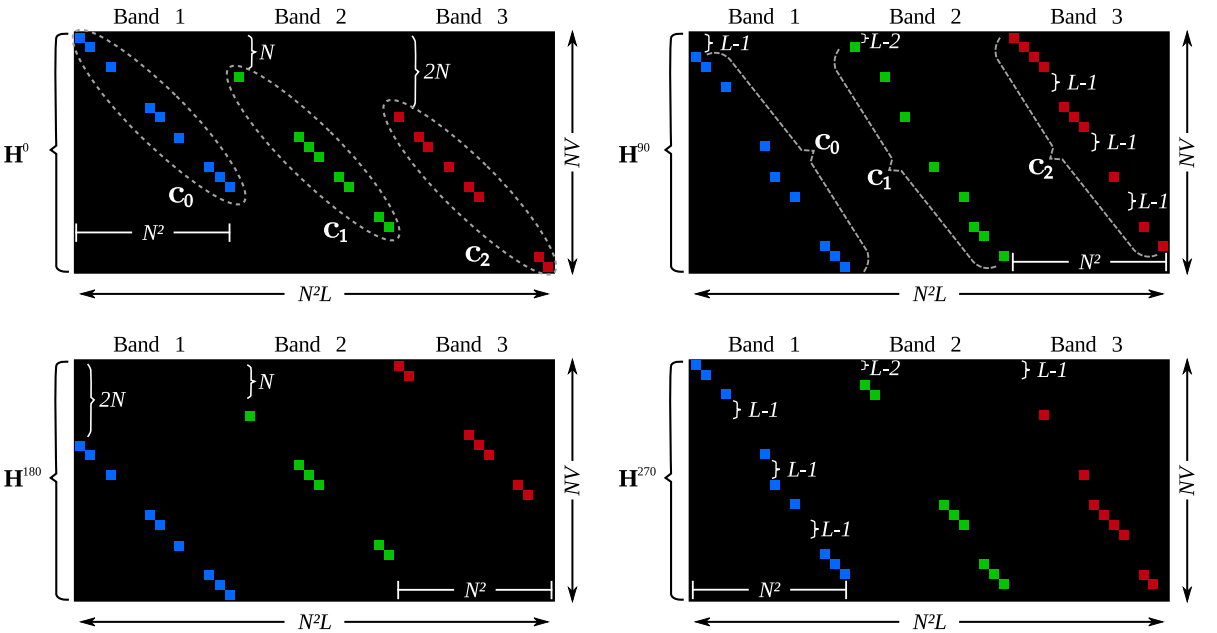

Fig. 4 Sensing matrix $\mathbf{H}^{\varphi}$ for $N = 4$, $L = 3$, and $\varphi = 0$, 90, 180, and 270 deg. The structure of each matrix accounts for the effects of the dispersion, coding, and integration processes occurring in the multishot SCCSI system for each applied rotation angle.

for $\ell = 0, \ldots, N^2L - 1$ and $j = 0, \ldots, NV - 1$, where $k = \lfloor \ell / N^2 \rfloor$, $w = N + 2L - 2$; $\tilde{N} = N^2 - N$; $\hat{N} = N^2 + N$; $\ell' = \ell - kN^2$; and $\mathbf{c} = [\mathbf{c}_0^{\mathrm{T}}, \mathbf{c}_1^{\mathrm{T}}, \ldots, \mathbf{c}_{L-1}^{\mathrm{T}}]^{\mathrm{T}}$ is the vector representation of the optical filter array $\mathbf{C}$, with $\mathbf{c}_k = [C_{0,0,k}, C_{1,0,k}, \ldots, C_{0,1,k}, \ldots, C_{(W-1),(W-1),k}]^{\mathrm{T}}$. Examples of the sensing matrices $\mathbf{H}^{\varphi}$ for a $N \times N \times L$ data cube with $N = 4$, $L = 3$ and are shown in Fig. 4. The measurement vectors $\mathbf{g}^{\varphi}$ acquired with each prism rotation can be succinctly expressed in vector form as $\mathbf{g} = [(\mathbf{g}^0)^T, (\mathbf{g}^{90})^T, (\mathbf{g}^{180})^T, (\mathbf{g}^{270})^T]^T$. Therefore, Eq. (7) can be rewritten in the standard form of an underdetermined system of linear equations

$$\mathbf{g} = \mathbf{H}\mathbf{f}, \tag{12}$$

where $\mathbf{H} = [(\mathbf{H}^0)^T, (\mathbf{H}^{90})^T, (\mathbf{H}^{180})^T, (\mathbf{H}^{270})^T]^T$ is the concatenation of all sensing matrices $\mathbf{H}^{\varphi}$.

2.4 *Reconstruction Process*

Given that the amount of acquired measurements $KN(N + L - 1)$, where K is the number of measurement shots, is far less than the number of 3-D data cube entries to be estimated N^2L, the reconstruction problem to be solved becomes ill posed; therefore, it cannot be solved by directly inverting the system in Eq. (12). The theory of compressive sensing provides an alternative method to recover the underlying spectral scene $\mathbf{f}$ from the measurement set $\mathbf{g}$, assuming that $\mathbf{f} \in \mathbb{R}^{N^2L}$ has a S-sparse representation in a given basis $\mathbf{\Psi}$ and there exists high incoherence between the sensing matrix $\mathbf{H}$ and the basis $\mathbf{\Psi}$. Therefore, the measurement set $\mathbf{g}$ in Eq. (12) can be expressed as $\mathbf{g} = \mathbf{H}\mathbf{\Psi}\boldsymbol{\theta}$, where $\mathbf{f} = \mathbf{\Psi}\boldsymbol{\theta}$ and $\boldsymbol{\theta}$ is a sparse vector with $S \ll N^2L$ nonzero entries, such that $\mathbf{f}$ can be approximated as a linear combination of only S columns of $\mathbf{\Psi}$. Then, the inverse CS problem consists of recovering $\boldsymbol{\theta}$ so the $\ell_2 - \ell_1$ cost function is minimized, i.e., it looks for a sparse approximation of the spatio-spectral data cube. Mathematically, the optimization problem can be written as $\mathbf{f} = \mathbf{\Psi}\left\{ \arg\min_{\boldsymbol{\theta} \in \mathbb{R}^{N^2L}} \|\mathbf{g} - \mathbf{H}\mathbf{\Psi}\boldsymbol{\theta}\|_2 + \tau\|\boldsymbol{\theta}\|_1 \right\}$, where τ is a regularization constant.

3 Simulations

Three spectral data cubes $\mathbf{F}$, with spatial resolution of 256×256 pixels and $L = 8$ spectral bands in the range 400 to 700 nm were used to perform simulations to analyze the performance of the proposed multishot SCCSI approach. The first test database was obtained by illuminating the scene with a monochromatic light source.[12] Figure 5(a) shows the spectral bands of this test data cube at their central wavelengths. The second database is an indoor scene acquired under daylight illumination,[27] and the third data cube is a color palette.[28] Figures 5(b) and 5(c) show an RGB representation of the second and third databases, respectively.

In general, coding patterns employed in CSI architectures are designed so a 50% transmittance is achieved. In other words, half of their elements are blocking and half let the light pass through. This configuration allows reliable reconstructions.[20] Therefore, the sensing process of the multishot SCCSI system was simulated using a predefined set of different optical filters whose bandpass spans half of the spectral bandwidth of $\mathbf{F}$. The optical filters are randomly distributed within the optical filter array $\mathbf{C}$, following a uniform distribution; hence, a 50% transmittance of the overall optical filter array is guaranteed. To obtain a suitable spectral reconstruction, the selected set of optical filters must uniformly sense information from all spectral bands. Figure 6 shows the set of eight predefined filters employed. Simulations were performed varying the number of optical filters from two to eight, which match the number of spectral bands, to determine the effect produced in the reconstructed image quality. Also, the number of snapshots varies from

Downloaded From: http://opticalengineering.spiedigitallibrary.org/ on 03/03/2017 Terms of Use: http://spiedigitallibrary.org/ss/termsofuse.aspx

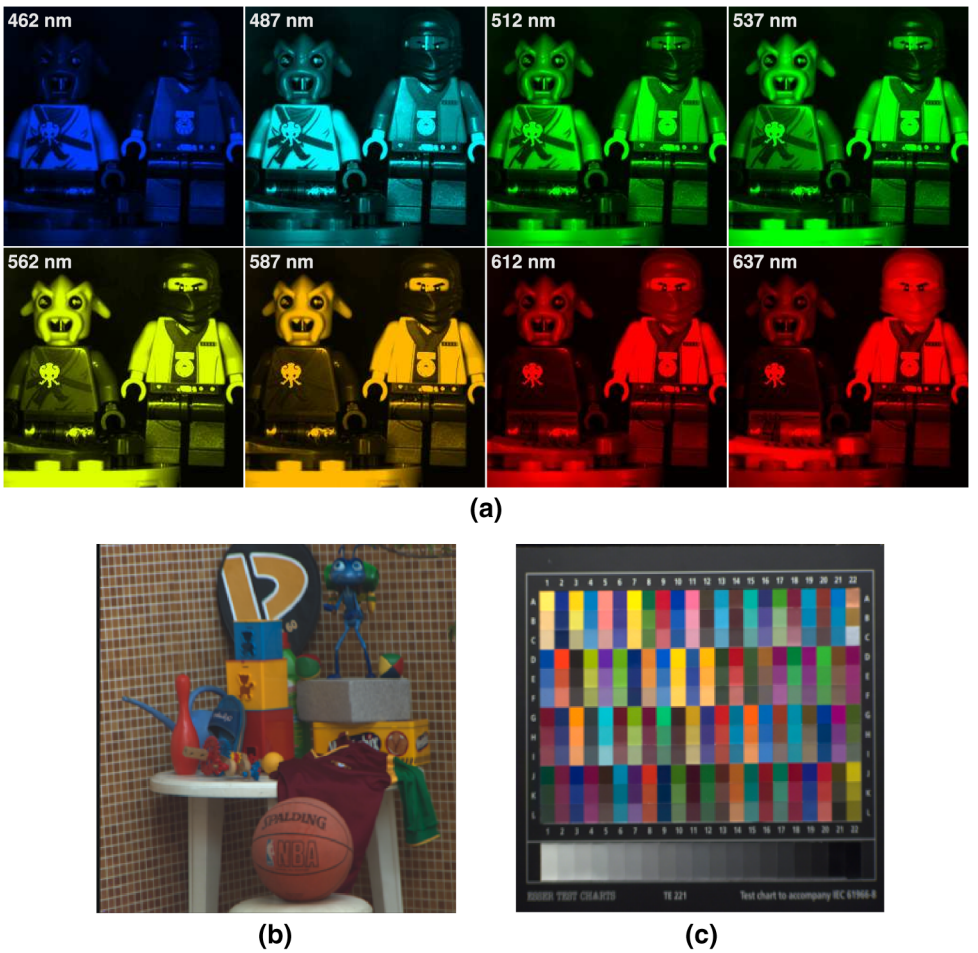

Fig. 5 Test data cubes used for simulations. Each data cube has spatial resolution of 256×256 pixels and eight spectral bands ranging from 400 (λ_1) to 700 nm (λ_8). (a) Spectral bands with central wavelengths of the first data cube; (b) RGB representation of the indoor scene data cube; and (c) RGB representation of the color palette data cube.

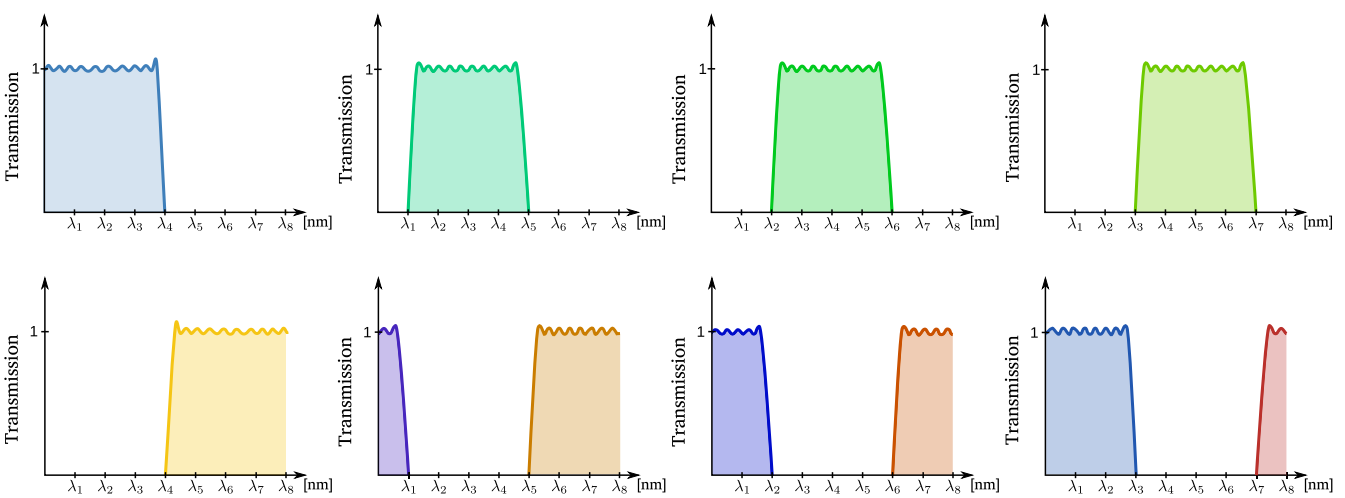

Fig. 6 Set of predefined bandpass optical filters used for simulations. The bandwidth of the optical filters corresponds with an overall 50% transmittance of the color filter array. Such transmittance is guaranteed when these filters are uniformly distributed in **C**.

Downloaded From: http://opticalengineering.spiedigitallibrary.org/ on 03/03/2017 Terms of Use: http://spiedigitallibrary.org/ss/termsofuse.aspx

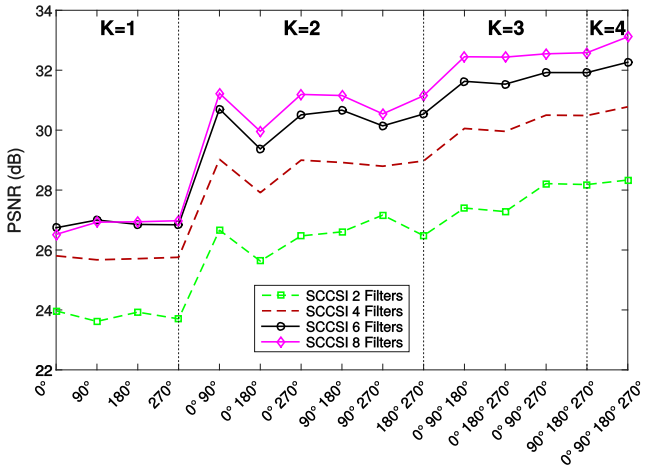

Fig. 7 Evaluation of all possible angle combinations for a specific number of measurement shots K. Note that all angle combinations for a given K provide similar PSNR results, thus it is possible to select any angle combination without a significant loss of quality in the reconstructions.

$K = 1$ to $K = 4$, which corresponds to the four selected rotation angles.

Compressive measurements for each data cube are acquired using Eqs. (5) and (6) corresponding to the rotations 0, 90, 180, and 270 deg. The simulated set of compressive measurements, the sensing matrix $\mathbf{H}$ obtained with Eqs. (8)–(11), and a regularization constant τ were used as inputs to a compressed sensing reconstruction algorithm to obtain the reconstruction of the spectral source. In particular, the results were attained using the gradient projection for sparse reconstruction (GPSR) algorithm.[29] The sparsifying basis is set to be a Kronecker product between a 2-D Wavelet Symmlet 8 basis for the spatial dimensions and a one-dimensional DCT basis for the spectral domain, $\mathbf{\Psi} = \mathbf{\Psi}_{\mathrm{2DW}} \otimes \mathbf{\Psi}_{\mathrm{DCT}}$. The results are compared with reconstructions obtained from the CASSI multishot system using binary coded apertures with 50% transmittance, whose entries follow a Bernoulli distribution.[10,23] Since random coding patterns were used in both SCCSI and CASSI system simulations, the presented results are the average of several experiments, each with a different random coding pattern.

The proposed multishot SCCSI model can capture at most $K = 4$ measurements shots since the described mathematical sensing model only considers the prism rotation at $\varphi = \{0, 90, 180, 270\}$ deg. However, $\binom{4}{K}$ different angle combinations can be taken for a given number of measurement shots, K. For instance, for $K = 1$, the set of compressive measurements can be acquired by rotating the prism to any of the four possibilities: $\varphi = 0$ deg, $\varphi = 90$ deg, $\varphi = 180$ deg, or $\varphi = 270$ deg. For this reason, the first experiment consists of evaluating the reconstruction quality for each possible angle combination. Figure 7 shows the peak signal-to-noise ratio (PSNR) obtained for all possible angle combinations for the different number of shots K. These results show that for a given K, all combinations result in similar reconstruction quality; thus, there is not a specific angle combination that provides a significantly better PSNR. Therefore, subsequent experiments are performed using a single angle combination for each K. Specifically, for $K = 1$, the sensing process will be simulated applying a $\varphi = 0$ deg prism rotation; for $K = 2$, the prism will be rotated to $\varphi = \{0, 90\}$ deg; for $K = 3$ the prism will be rotated to $\varphi = \{0, 90, 180\}$ deg; and for $K = 4$, the prism will be rotated to $\varphi = \{0, 90, 180, 270\}$ deg.

Figure 8 shows a comparison between the average reconstruction PSNR obtained with the SCCSI and CASSI multishot systems for the three data bases, varying the number of shots from $K = 1$ to $K = 8$, which correspond to compression ratios from 1/8 to 1. In general, the SCCSI multishot system outperforms the results obtained with CASSI providing a gain up to 5 dB in PSNR. In addition, it can be observed that the proposed approach always improves the results obtained with CASSI using $K \leq 4$ measurement shots and only four optical filters in the detector. Furthermore, the obtained results for the first and second databases show that with $K = 4$ measurement shots and six optical filters in the detector, SCCSI outperforms the CASSI result even using more than $K = 6$ measurement shots. On the other hand, it can also be observed that taking multiple measurement shots improves the results obtained with SCCSI single shot since more compressive measurements are acquired. Specifically, with only $K = 2$ measurement shots, the proposed system provides an improvement of up to 4 dB in PSNR. Furthermore, for $K = 4$, a gain up

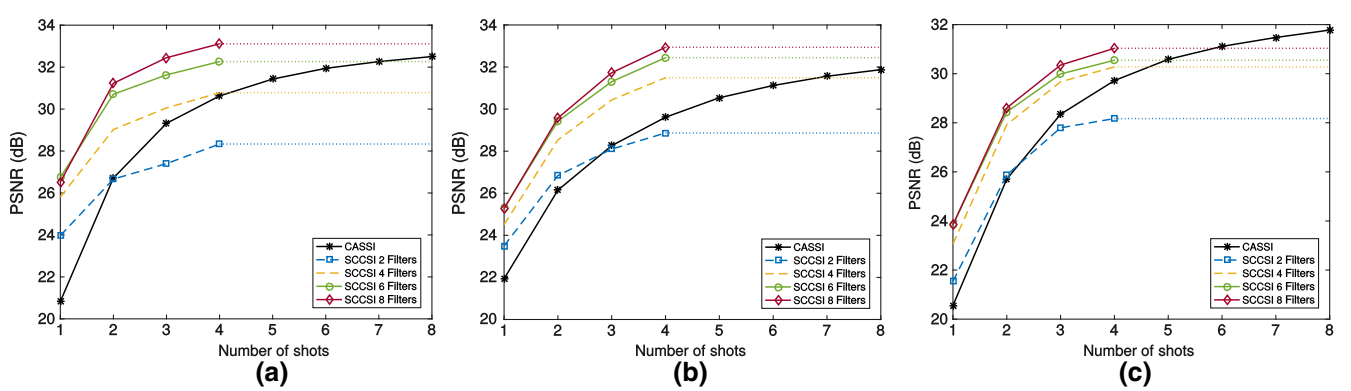

Fig. 8 Average reconstruction PSNR as a function of the number of shots using CASSI and SCCSI multishot systems, varying the number of optical filters in the SCCSI detector between two and eight for (a) data cube in Fig. 5(a), (b) indoor scene in Fig. 5(b), and (c) color palette in Fig. 5(c).

Downloaded From: http://opticalengineering.spiedigitallibrary.org/ on 03/03/2017 Terms of Use: http://spiedigitallibrary.org/ss/termsofuse.aspx

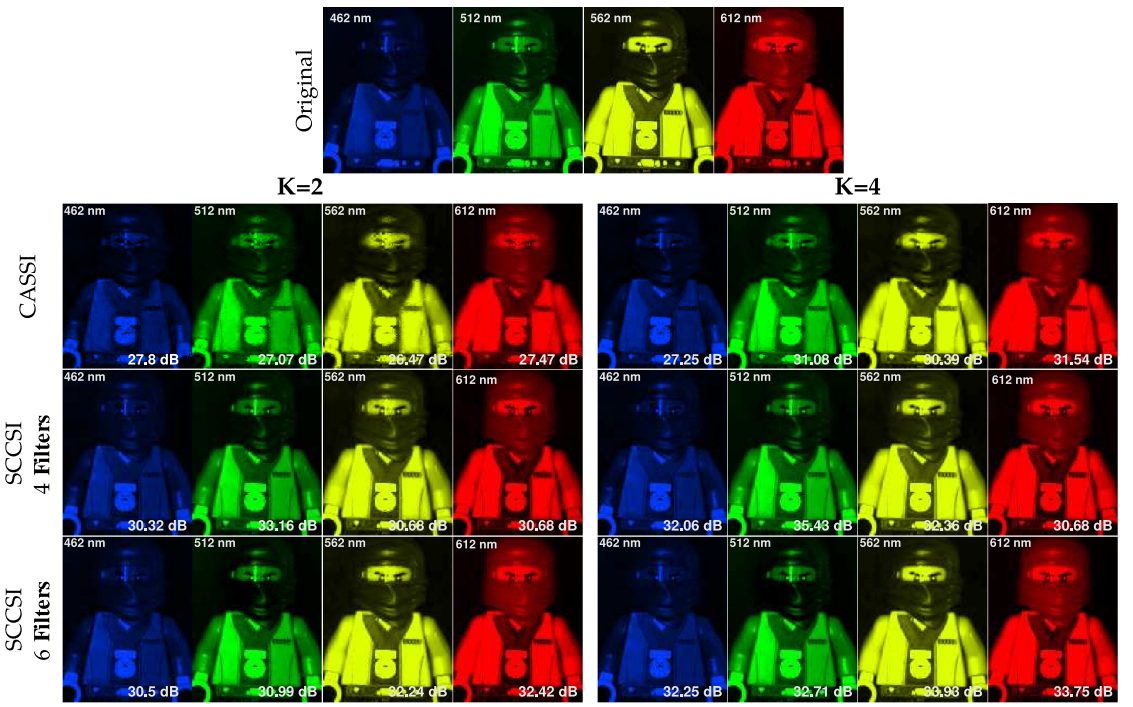

Fig. 9 Zoomed reconstruction of the spectral bands $\lambda_1 = 462$ nm, $\lambda_3 = 512$ nm, $\lambda_5 = 562$ nm, and $\lambda_7 = 612$ nm using CASSI, SCCSI with four filters, and SCCSI with six filters and $K = 2$, 4 measurement shots.

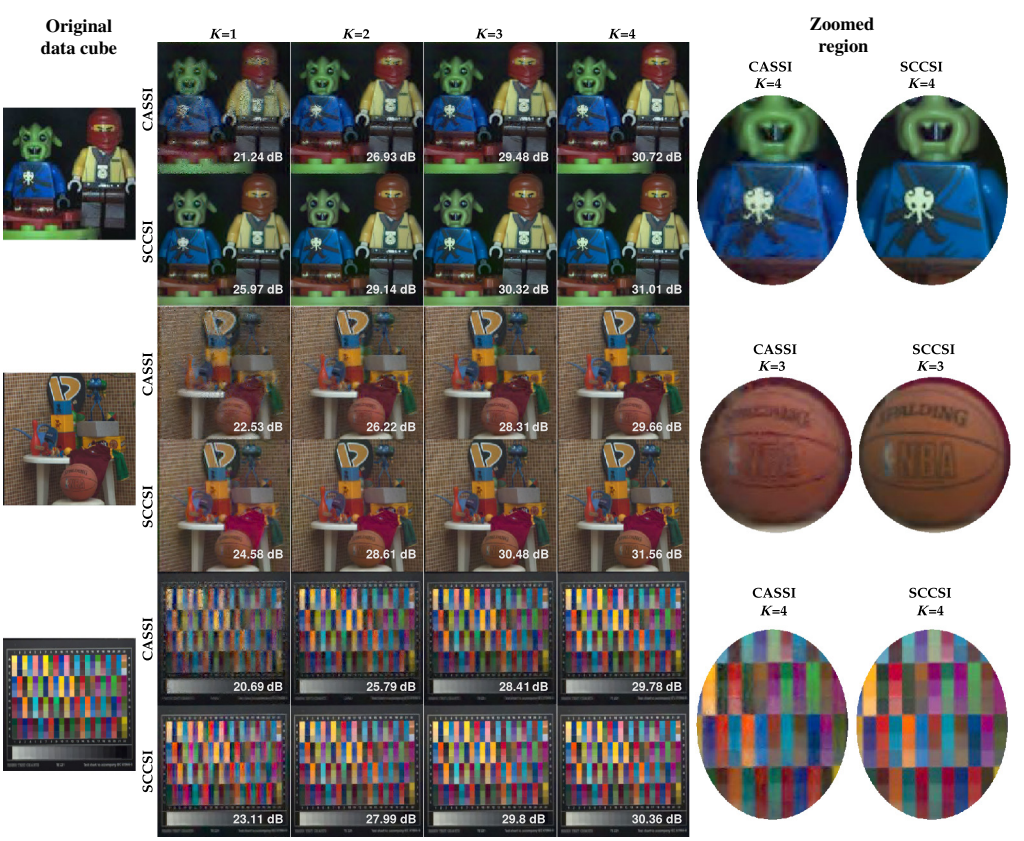

Fig. 10 RGB mapping of the recovered data cubes using CASSI and SCCSI with four optical filters in the detector and a different number of snapshots. The zoomed regions illustrate the improvements in the reconstructed details attained with the multishot SCCSI approach.

Downloaded From: http://opticalengineering.spiedigitallibrary.org/ on 03/03/2017 Terms of Use: http://spiedigitallibrary.org/ss/termsofuse.aspx

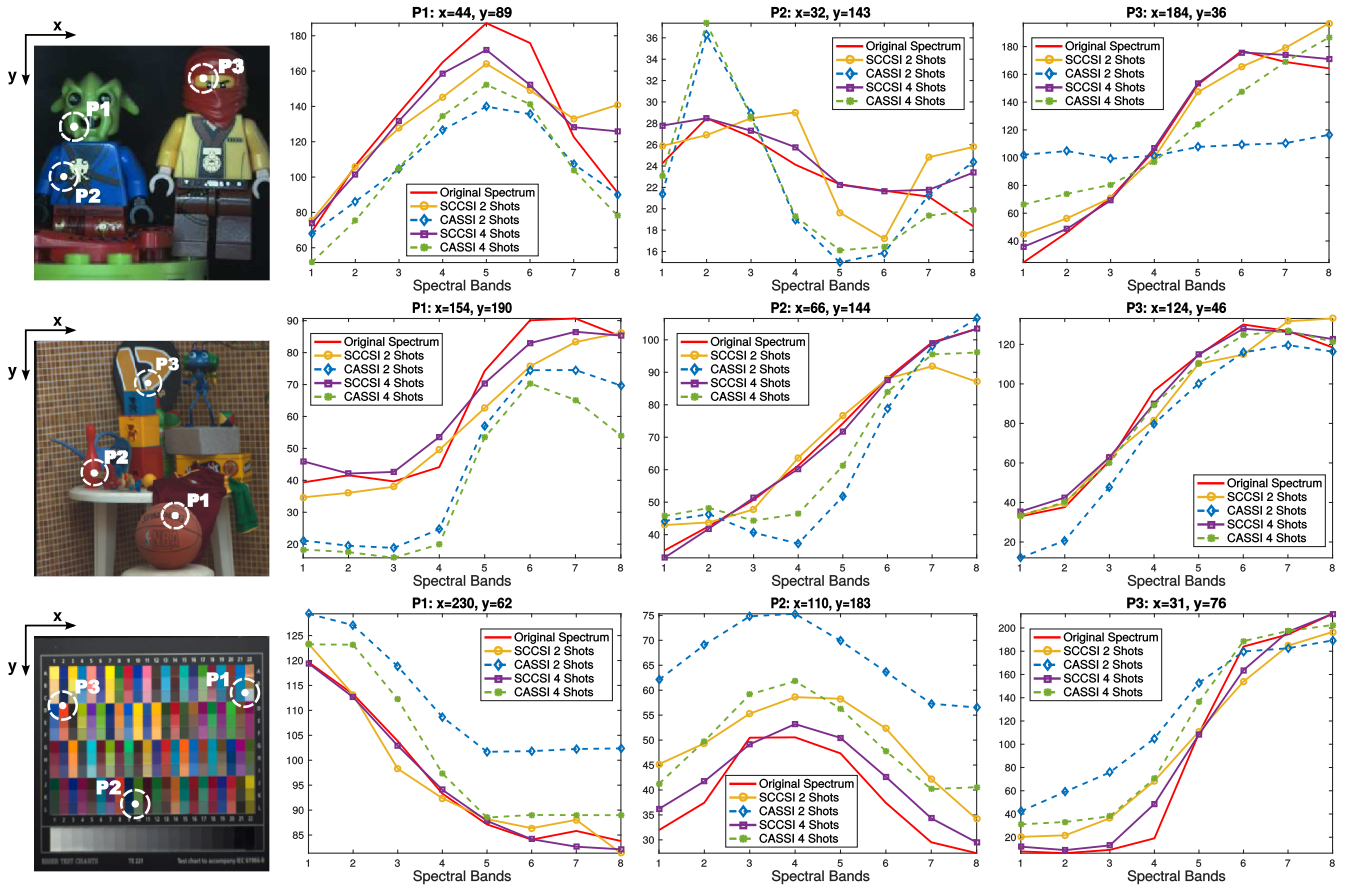

Fig. 11 Reconstructions along the spectral axis for highlighted spatial locations in the three test data cubes using $K = 2$, 4 measurement shots in both CASSI and SCCSI with four optical filters.

to 7 dB in PSNR is obtained. In general, it can be seen that increasing the number of optical filters leads to an improvement in the SCCSI reconstruction PSNR. However, increasing the number of filters in the detector to more than five does not represent a significant gain in the reconstruction PSNR of eight spectral bands.

Figure 9 shows the reconstructions of a subset of spectral bands from the first data cube, using $K = 2$, 4 snapshots of CASSI and SCCSI with four and six filters in the detector. These results show that, with two measurement shots and four filters in the detector, the SCCSI architecture provides more detailed reconstructions than CASSI. Figure 10 shows the RGB representation of all the reconstructed data cubes for $K = 1$ to $K = 4$ measurement shots using CASSI and SCCSI with four optical filters in the detector. The zoomed regions in Fig. 10 show the improvements attained with the multishot SCCSI system with respect to multishot CASSI.

To verify the accuracy of the proposed multishot SCCSI approach, Fig. 11 shows the spectral signatures for three spatial points in the reconstructions obtained from CASSI and SCCSI with four filters, randomly distributed at the detector, using $K = 2$, 4 measurement shots in both architectures. These results show that the SCCSI spectral reconstructions are more accurate than those of the CASSI architecture. Furthermore, increasing the number of measurement shots results in more accurate spectral reconstructions for both architectures.

4 Conclusions

The multishot SCCSI has been presented. The mathematical model for the multishot SCCSI was developed. The proposed approach allows the acquisition of multiple snapshots using the SCCSI optical architecture, which does not admit coding pattern variation as other CSI architectures. The proposed approach consists of rotating the dispersive element of the original architecture such that the dispersion direction depends on the rotation angle and the input source is encoded at different detector regions. In addition, this approach employs the same optical elements of the SCCSI original architecture. Taking multiple snapshots leads to improved spatial and spectral reconstructions. Simulations show that a gain of up to 7 dB is attained when four measurement shots are compared to the original single snapshot SCCSI. Furthermore, multishot SCCSI overcomes both the spatial and spectral reconstructions attained with the state-of-the-art CSI architecture, the CASSI system, even when a low number of optical filters is used. Moreover, an improvement of up to 5 dB of PSNR is obtained with respect to the CASSI system.

Acknowledgments

The authors gratefully acknowledge the Vicerrectoría de Investigación y Extensión of Universidad Industrial de Santander for supporting this work registered under the project titled “Diseño y simulación de un sistema adaptativo

Downloaded From: http://opticalengineering.spiedigitallibrary.org/ on 03/03/2017 Terms of Use: http://spiedigitallibrary.org/ss/termsofuse.aspx

de sensado compresivo de secuencias de video espectral," (VIE code 1891). Claudia V. Correa is supported by a Colciencias scholarship.

References

1. L. Gao et al., "Snapshot image mapping spectrometer (IMS) with high sampling density for hyperspectral microscopy," *Opt. Express* **18**(14), 14330–14344 (2010).
2. A. Bodkin, A. Sheinis, and A. Norton, "Hyperspectral imaging systems," U.S. Patent App. 11/220, 016 (2005).
3. A. R. Harvey et al., "Imaging spectrometry at visible and infrared wavelengths using image replication," *Proc. SPIE* **5612**, 190 (2004).
4. B. Geelen et al., "Low-complexity image processing for a high-throughput low-latency snapshot multispectral imager with integrated tiled filters," *Proc. SPIE* **8743**, 87431E (2013).
5. J. M. Eichenholz and J. Dougherty, "Ultracompact fully integrated megapixel multispectral imager," *Proc. SPIE* **7218**, 721814 (2009).
6. J. M. Eichenholz et al., "Real-time megapixel multispectral bioimaging," *Proc. SPIE* **7568**, 75681L (2010).
7. Y. Murakami, M. Yamaguchi, and N. Ohyama, "Hybrid-resolution multispectral imaging using color filter array," *Opt. Express* **20**(7), 7173–7183 (2012).
8. G. R. Arce et al., "Compressive coded aperture spectral imaging: an introduction," *IEEE Signal Process Mag.* **31**(1), 105–115 (2014).
9. D. Brady and M. Gehm, "Compressive imaging spectrometers using coded apertures," *Proc. SPIE* **6246**, 62460A (2006).
10. A. Wagadarikar et al., "Single disperser design for coded aperture snapshot spectral imaging," *Appl. Opt.* **47**(10), B44–B51 (2008).
11. H. Arguello and G. R. Arce, "Rank minimization code aperture design for spectrally selective compressive imaging," *IEEE Trans. Image Process.* **22**(3), 941–954 (2013).
12. C. V. Correa, H. Arguello, and G. R. Arce, "Snapshot colored compressive spectral imager," *J. Opt. Soc. Am. A* **32**(10), 1754–1763 (2015).
13. S. Kim et al., "Multifocusing and depth estimation using a color shift model-based computational camera," *IEEE Trans. Image Process.* **21**(9), 4152–4166 (2012).
14. J. Barrie et al., "Patterning of multilayer dielectric optical coatings for multispectral CCDs," *Thin Solid Films* **270**(1), 6–9 (1995).
15. P. Stupar et al., "MEMS tunable Fabry-Perot filters with thick, two sided optical coatings," in *Int. Solid-State Sensors, Actuators and Microsystems Conf. (TRANSDUCERS '09)*, pp. 1357–1360, IEEE (2009).
16. D. Hays et al., "A hybrid MEMS–fiber optic tunable Fabry–Perot filter," *J. Microelectromech. Syst.* **19**(2), 419–429 (2010).
17. Y. Bando, B.-Y. Chen, and T. Nishita, "Extracting depth and matte using a color-filtered aperture," *ACM Trans. Graph.* **27**(5), 134 (2008).
18. D. L. Donoho, "Compressed sensing," *IEEE Trans. Inf. Theory* **52**(4), 1289–1306 (2006).
19. H. Arguello, Y. Mejia, and G. Arce, "Colored coded apertures optimization in compressive spectral imaging by restricted isometry property," in *IEEE Int. Conf. on Image Processing (ICIP '14)*, pp. 600–604, IEEE (2014).
20. H. Arguello and G. R. Arce, "Restricted isometry property in coded aperture compressive spectral imaging," in *IEEE Statistical Signal Processing Workshop (SSP '12)*, pp. 716–719, IEEE (2012).
21. D. Kittle et al., "Multiframe image estimation for coded aperture snapshot spectral imagers," *Appl. Opt.* **49**(36), 6824–6833 (2010).
22. H. Arguello and G. R. Arce, "Code aperture optimization for spectrally agile compressive imaging," *J. Opt. Soc. Am. A* **28**(11), 2400–2413 (2011).
23. Y. Wu et al., "Development of a digital-micromirror-device-based multishot snapshot spectral imaging system," *Opt. Lett.* **36**(14), 2692–2694 (2011).
24. H. Arguello and G. Arce, "Code aperture design for compressive spectral imaging," in *18th European Signal Processing Conf.*, pp. 1434–1438, IEEE (2010).
25. C. A. Hinojosa et al., "Compressive spectral imaging using multiple snapshot colored-mosaic detector measurements," *Proc. SPIE* **9870**, 987004 (2016).
26. R. Deming et al., "Robust detection and spectrum estimation of multiple sources from rotating-prism spectrometer images," *Proc. SPIE* **6365**, 636502 (2006).
27. D. H. Foster et al., "Frequency of metamerism in natural scenes," *J. Opt. Soc. Am. A* **23**(10), 2359–2372 (2006).
28. G. D. Finlayson, S. D. Hordley, and P. Morovic, "Using the spectracube to build a multispectral image database," in *Conf. on Colour in Graphics, Imaging, and Vision*, Vol. 2004, No. 1, pp. 268–274, Society for Imaging Science and Technology (2004).
29. M. A. Figueiredo, R. D. Nowak, and S. J. Wright, "Gradient projection for sparse reconstruction: application to and other inverse problems," *IEEE J. Sel. Top. Signal Process.* **1**(4), 586–597 (2007).

Claudia V. Correa received her BE degree in computer science in 2009 and her MSc degree in systems engineering in 2013 from the Universidad Industrial de Santander (UIS), Colombia. She received her MSc degree in electrical engineering from the University of Delaware in 2013. She is currently a PhD candidate in the Electrical and Computer Engineering Department, University of Delaware, USA. Her research interests include compressive spectral imaging, computational imaging, and compressed sensing.

Carlos A. Hinojosa received his BE degree in computer science from the Universidad Industrial de Santander (UIS), Colombia, in 2015. He is currently a Msc candidate in the Computer Science Department at Universidad Industrial de Santander. His research interests include high-dimensional signal coding and processing, compressive spectral imaging, computational imaging, and compressive sensing.

Gonzalo R. Arce received his PhD in electrical engineering from Purdue University, USA. He is currently the Charles Black Evans professor of electrical and computer engineering with the University of Delaware, Newark. He was the Fulbright Nokia Distinguished Chair in Information and Communications Technologies with Aalto University, Finland, in 2010. He was an associate editor and guest editor of several journals of the IEEE, the Optical Society of America, and SPIE.

Henry Arguello received his BE degree in electrical engineering in 2000, and his MSc degree in electrical power in 2003 from the Universidad Industrial de Santander (UIS), Colombia. He received his PhD in electrical engineering from the University of Delaware, USA, in 2013. He is a professor at the Department of Systems Engineering, Universidad Industrial de Santander, Colombia. His research interests include high-dimensional signal processing, optical imaging, compressed sensing, hyperspectral imaging, and computational imaging.

Downloaded From: http://opticalengineering.spiedigitallibrary.org/ on 03/03/2017 Terms of Use: http://spiedigitallibrary.org/ss/termsofuse.aspx